Published in "Nature Materials 16(4): 467–473, 2017"
which should be cited to refer to this work.

Temporal mapping of photochemical reactions and molecular excited states with carbon specificity

K. Wang[1,2†], P. Murahari[2†], K. Yokoyama[2,3], J. S. Lord[3], F. L. Pratt[3], J. He[1], L. Schulz[1], M. Willis[1], J. E. Anthony[4], N. A. Morley[5], L. Nuccio[6], A. Misquitta[2], D. J. Dunstan[2], K. Shimomura[7], I. Watanabe[8], S. Zhang[1], P. Heathcote[9]* and A. J. Drew[1,2,3]*

Photochemical reactions are essential to a large number of important industrial and biological processes. A method for monitoring photochemical reaction kinetics and the dynamics of molecular excitations with spatial resolution within the active molecule would allow a rigorous exploration of the pathway and mechanism of photophysical and photochemical processes. Here we demonstrate that laser-excited muon pump–probe spin spectroscopy (photo-μSR) can temporally and spatially map these processes with a spatial resolution at the single-carbon level in a molecule with a pentacene backbone. The observed time-dependent light-induced changes of an avoided level crossing resonance demonstrate that the photochemical reactivity of a specific carbon atom is modified as a result of the presence of the excited state wavefunction. This demonstrates the sensitivity and potential of this technique in probing molecular excitations and photochemistry.

Dynamics of molecular excited states govern photochemical reactions that are key to a phenomenal number of important industrial and biological processes. For example, molecules in living organisms are often exposed to solar radiation, and in the case of photosynthesis this light energy is captured to provide the energy that supports almost all life. Moreover, the effect of this solar radiation on biomolecules such as DNA plays an important evolutionary role[1,2]. In the chemical engineering field, stereoselective synthesis enables the construction of a vast array of organic molecules with precise control over their three-dimensional structure[3,4], which is important in a variety of fields ranging from drug discovery to materials engineering. Photochemical reactions have a substantial impact on these fields by affording direct access to certain structural motifs that are otherwise difficult to construct[5]. For example, the malaria drug artemisinin is commercially produced with a key photochemical step[6]. In organic electronics, the complex physics of excitations is critical to device function[7–13]. High efficiencies have been reached for both organic light-emitting diodes (OLEDs) and organic photovoltaics (OPVs)[14–17], yet a major barrier to the deployment of organic semiconductors is their functional lifetime[17]. For example, a recent study of the chemical reactivity of derivatives of anthracene and tetracene in the OLED environment indicates that free-radical chemistry is initiated after photo-excitation by homolytic bond dissociation reactions, which result in hydrogenation reactions[18].

We have developed the experimental technique photo-μSR[19] so that it can now measure the spatial distribution of electron density in the molecular excited state at any given time. Whilst this technique has previously been used to study excitations predominantly in semiconductors[19,20] and a limited number of solutions of organic molecules[21], no spatial information has been gained up until now. By making use of avoided level crossing (ALC) spectroscopy, whose resonance positions are specific to individual carbons, we demonstrate that crucial information on the fundamental photochemical and excited state processes can be obtained. We demonstrate this new application of the technique in a 10 mM solution of the organic semiconductor 6,13-bis(tri(isopropyl)silylethynyl) pentacene (TIPS-Pn) (Fig. 1a), dissolved in O_2-free dichloromethane (DCM). We present convincing evidence that muonium is able to map the time evolution of the excited state wavefunction on the pentacene backbone of the molecule, as a direct result of its sensitivity to electron density when reacting. We demonstrate that reaction of muonium with this extended aromatic system probes the relative levels of chemical reactivity of carbon atoms after excitation with light, and that this can be tracked as a function of time.

Photo-μSR

In our photo-μSR experiment, a 25 Hz, ∼10 ns pulsed Nd:YAG laser was used to excite the TIPS-Pn molecules in solution with a wavelength of 532 nm and a pulse energy of 91 mJ. The light-pump muon-probe measurements were carried out on the HiFi spectrometer at the ISIS pulsed muon source, with the light flash triggered to arrive T_L before the muon pulse, to excite the TIPS-Pn molecules prior to the arrival of the muons, as depicted in Fig. 1b,c. The changes to the photochemical reaction rates as a result of the excitation can then be probed with muonium, a chemical analogue of hydrogen (see below). The 25 Hz laser in combination with the 50 Hz muon pulse enabled light-on/off data to be gated to alternate histograms, thus averaging out any long-term changes to

[1]College of Physical Sciences and Technology, Sichuan University, Chengdu, Sichuan 610064, China. [2]School of Physics and Astronomy, Queen Mary University of London, Mile End, London E1 4NS, UK. [3]ISIS Muon Facility, Rutherford Appleton Laboratory, Didcot OX11 0QX, UK. [4]Department of Chemistry, University of Kentucky, Lexington, Kentucky 40506, USA. [5]Department of Materials Science and Engineering, University of Sheffield, Sheffield S1 3JD, UK. [6]University of Fribourg, Department of Physics and Fribourg Centre for Nanomaterials, Chemin du Museé 3, CH-1700 Fribourg, Switzerland. [7]Materials and Life Science Division, J-PARC Center, Tokai, Ibaraki 319-1195, Japan. [8]RIKEN-RAL, Nishina Centre, 2-1 Hirosawa, Wako, Saitama 351-0198, Japan. [9]School of Biological and Chemical Sciences, Queen Mary University of London, Mile End, London E1 4NS, UK. †These authors contributed equally to this work. *e-mail: P.Heathcote@qmul.ac.uk; A.J.Drew@qmul.ac.uk

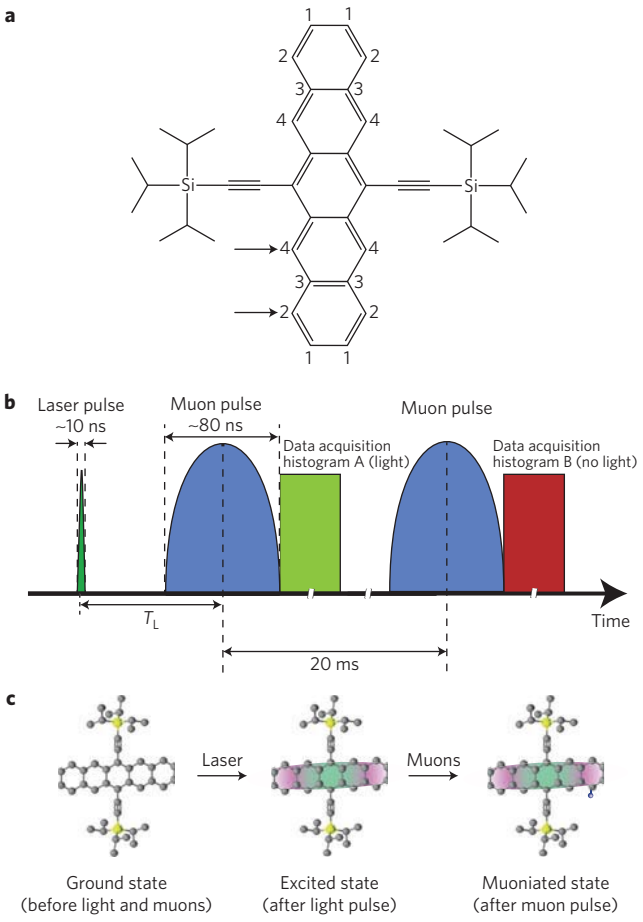

Figure 1 | A schematic illustration of the molecule under investigation and the experimental set-up. a, The molecular structure of TIPS-Pn. The labels are referred to in the text. Sites 1, 2 and 4 can support muonium bonding. All similarly numbered sites are equivalent, by symmetry. The arrows correspond to the muonium bonding positions that are probed as a function of delay time, in Fig. 2c. **b**, The pump–probe pulse structure in our experiments. The laser pulse (dark green) is triggered to arrive prior to the muon pulse (blue), and the delay time between the pulses, T_L, is controllable. The muon pulses are separated by 20 ms, which is determined by the ISIS synchrotron intrinsic frequency of 50 Hz, whereas the laser is fired at 25 Hz. The data are then gated to different histograms, depending on whether a laser pulse directly preceded the muon pulse or not. **c**, The different stages of the molecule during the experiment. TIPS-Pn starts out in the ground state, without a muon probe present. Upon excitation with light, an excited state is formed, as indicated by the green and pink shading, which is subsequently probed with a muonium that bonds to one of the carbons.

the sample and accelerator profile. Further technical details can be found elsewhere[19,22], in the Methods and in the Supplementary Information.

When implanted into many materials including organic solvents, the positively charged muons can either thermalize as diamagnetic species or form hydrogen-like muonium atoms, Mu (ref. 22). Mu is thought of as a light pseudo-isotope of the hydrogen atom, in which an electron orbits a muon (μ^+) nucleus, which is 0.11 the mass of H and behaves chemically like a H atom[22–26]. Due to the unsaturated bonds and aromatic rings that are present, muonium can react with TIPS-Pn with almost identical chemistry to a hydrogen atom, creating an electrically neutral radical. There are three species of muon in our sample, a diamagnetic and two types of paramagnetic species: the unbound solvated species with a hyperfine coupling (HFC) constant of order 4.4 GHz, and a number of muoniated radicals, which have a significantly lower HFC constant for the muon and other nuclei in the molecule that are dependent on their local environment.

Indeed, it is these differences in HFCs that depend on the muon's local environment which give us spatial sensitivity. The unpaired electron wavefunction in a radical overlaps with the nuclei and gives a series of hyperfine coupling constants for all the nuclei with non-zero spin, which are generally much lower than for the individual free atoms. In the simpler case of gases, liquids or solutions, only the isotropic parts of the coupling constants need be considered. When a magnetic field is applied parallel to the muon's initial spin polarization, the spin energy levels are split by the Zeeman interaction. At certain fields, the combination of Zeeman and hyperfine interactions cause cross-relaxation between the muon and one of the other nuclei, and a so-called ALC resonance[22,27–29].

These resonances are usually plotted as the 'integral asymmetry'—the average muon polarization weighted by the muon lifetime, and take the form of relatively sharp dips. The amplitude of the integral ALC resonance depends on the hyperfine coupling of both muon and nucleus. In many aromatic molecules each radical species has one dominant resonance due to the α-proton. The amplitude and width are also affected by relaxation and other dynamics, and the formation rate and probability of that species. ALCs from different radical species caused by different addition sites of the muonium will generally be at quite different fields, so they can be measured individually. Importantly, one of the main drivers of the relative amplitude of the various ALC resonances is the reaction kinetics associated with muonium bonding. That is itself driven by the electrostatic potential, which of course can be quite different when the molecule is in the ground state compared to an excited state. We show that our photo-μSR experiment can spatially probe the molecular excited state and its role in determining reactivity of the molecule, all at an individual atom level. Moreover, by changing the pump–probe delay time, T_L, temporal information is obtained as the transient excited species evolves with time.

Light-induced effects on ALC spectra

Figure 2a shows the ALC spectra taken for muonium bound to carbons 1, 2 and 4 in TIPS-Pn at $T_L = 130$ ns. The laser and muon pulse are sufficiently separated to ensure that photo-ionization of muonium or muoniated radicals could not occur[30]. Figure 2b shows the ALC from muon–electron and muon–proton (α-proton) HFCs predicted from *ab initio* density functional theory (DFT) calculations, which can be used to assign the bonding site for each ALC resonance. The site assignment is in the inset. Further details of these DFT calculations can be found in the Supplementary Information. It is immediately clear that photo-excited changes to the spectra are evident for sites 1 and 2 but not site 4. The largest changes are evident at site 2, with a clear increase in amplitude, or area of the ALC, as well as a small shift in the ALC minima (potentially as a result of a HFC change). There could be an increase in the width of the lines for both sites 1 and 2, although this is difficult to quantify since these ALCs overlap. Figure 2c inset shows the light-induced change in asymmetry, A_{diff}, as a function of T_L, at two fixed fields (indicated by the arrows in Fig. 2a), corresponding to sites 2 and 4 (indicated by the arrows in Fig. 1a). There are two components present corresponding to ALC spectral changes at site 2, with different signs and timescales, that are not present at site 4. The 6.5 μs lifetime of the triplet molecular excited state is clearly evident in the slower component—strong evidence that muonium is directly detecting the presence of triplet excited states. The ALC amplitude of this component is reduced in the triplet state. The faster component, with an increased ALC amplitude, has a timescale of approximately 1 μs.

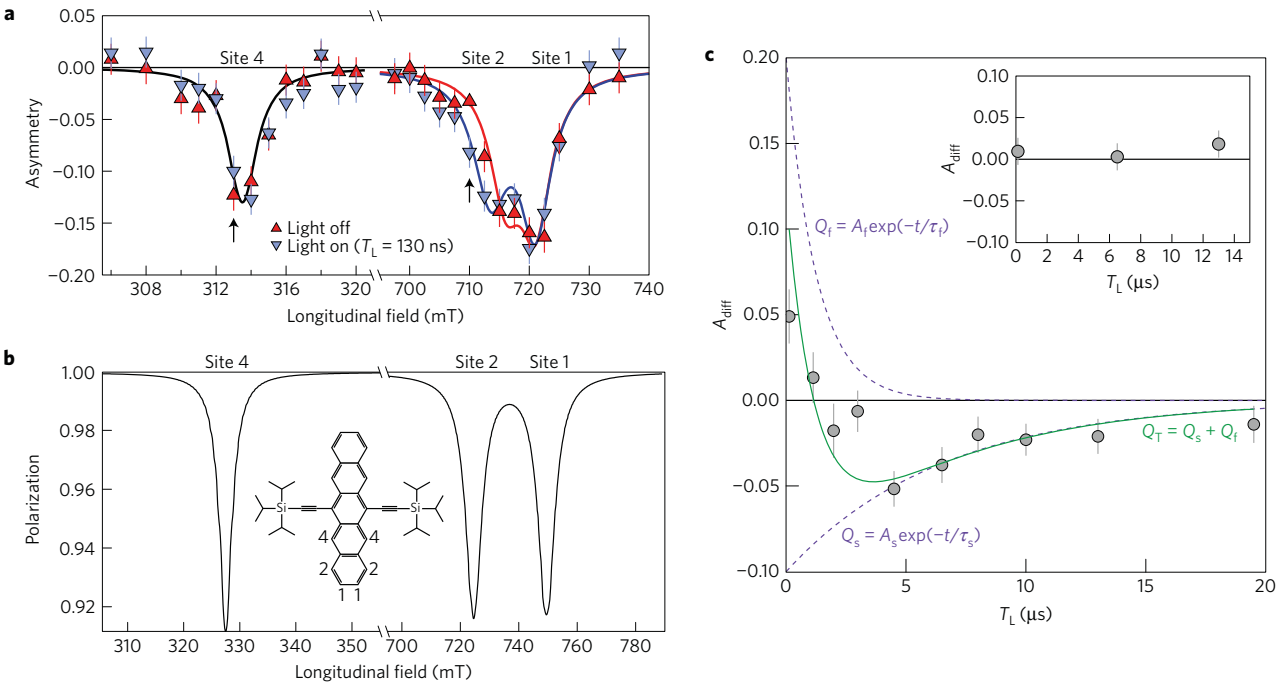

Figure 2 | The time-dependent ALC measurements. a, ALC spectra with light off (red) and light on (blue) with a pump–probe time delay of 130 ns. There is a clear light-induced change in shape of the two ALCs corresponding to sites 1 and 2, manifesting itself predominantly as a shift in position and an increase in amplitude/area, with the largest changes evident for site 2. The arrows correspond to the fixed fields that were measured as a function of T_L. **b**, Predicted lineshapes from DFT calculations (see Supplementary Information), from which site assignments can be made. The ALC at around 310 mT corresponds to site 4, whereas there are two ALCs that partially overlap at around 710 mT, corresponding to sites 1 and 2. **c**, The pump–probe delay time dependence of the change in amplitude of the ALC at 710 mT, $A_{diff} = A_{off} - A_{on}$. There are two timescales present, one at $\tau_f = 1\,\mu s$ and a second at $\tau_s = 6.5\,\mu s$, with opposite signs to the amplitudes A_f and A_s. Lines are guides to the eye, with the lifetimes fixed to values from transient photoabsorption measurements at 1.6 eV and 1.25 eV for τ_f and τ_s, respectively[35]. We note that the statistical error bars as plotted are significantly larger than any systematic errors in this measurement, which is reinforced by the similarity between the two lifetimes derived from the photo-μSR data, and those extracted from the transient photoabsorption data. Inset: Corresponding data on the ALC at 314 mT, where there appears to be no change in the ALC as a function of time. Where shown, in all panels, errors were calculated by taking the square root of the number of events for each detector group, and propagated using standard error analysis under the assumption of the normal distribution.

Light-induced changes to the ALC spectra can take many forms—for example, additional resonances could appear or ALC positions could shift, due to the presence of a distribution of unpaired spin on the molecule[19]. There could be a change in hyperfine coupling constant due to a structural or conformational difference[31], an increased electron spin relaxation or exchange[32–34], or a modification of the muonium reaction rate for a given carbon[31]. It is extremely unlikely that a conformational change or unpaired spin can account for this data, as the ALC at around 300 mT for site 4 is identical for the light-on and light-off cases. Either conformational or unpaired spin changes would modify the muon–electron and/or proton–electron isotropic hyperfine coupling (HFC) for all adducts[31]. For the same reasons, we also discount localized heating as a result of absorption of the light, since a relatively small change in temperature is known to significantly alter the position of the ALC for site 4 (see Supplementary Fig. 4). We also believe that electron spin relaxation and/or spin exchange cannot account for these changes—as it is known to affect all ALCs in a similar fashion in the solid state[32,33], there is no associated increase in relaxation rate and it cannot account for all of the features in the time-dependent data (see the Supplementary Information). To explain our observations, one must invoke the mechanism of radical formation from the solvated muonium. Muons thermalize very quickly, in less than 1 ns (ref. 22), with the final result in fully saturated organic solvents being a mixture of solvated muonium and unresolved diamagnetic muon states. The muonium then chemically reacts with the unsaturated or aromatic solute molecules, and if this final stage is not sufficiently prompt, then a number of features are observed in the data, which evolve with the reaction rate. These features, discussed below, are not present in the other candidate mechanisms mentioned above.

Interpreting the ALC spectra

In a weak transverse field (WTF), the energy differences between the two triplet transitions

$$|m_\mu, m_e\rangle = |1/2, 1/2\rangle \rightarrow (|1/2, -1/2\rangle + |-1/2, 1/2\rangle)/\sqrt{2}$$

and

$$(|1/2, -1/2\rangle + |-1/2, 1/2\rangle)/\sqrt{2} \rightarrow |-1/2, -1/2\rangle$$

are equal and relatively small, resulting in low-frequency Rabi oscillations[22,27]. The WTF spectra shown in Fig. 3a,b demonstrate a clear triplet precession signal (fast oscillation) superimposed on the precession from the diamagnetic muons (slow oscillation). The triplet precession results from muonium that stop in the unbound state, either in the SiO_2 window or the solvent. For muoniated radicals, the magnetic field at which the Zeeman splitting becomes nonlinear (that is, the two triplet transitions have a different energy) is significantly lower and the proton coupling splits the triplet energy difference. Given there are multiple radical states with different muon–electron and proton–electron HFC, the resulting signal is rather more complex, comprising of a superposition of multiple beating signals. We note that this will be also true for muonium addition to the triple bond of the sidegroup,

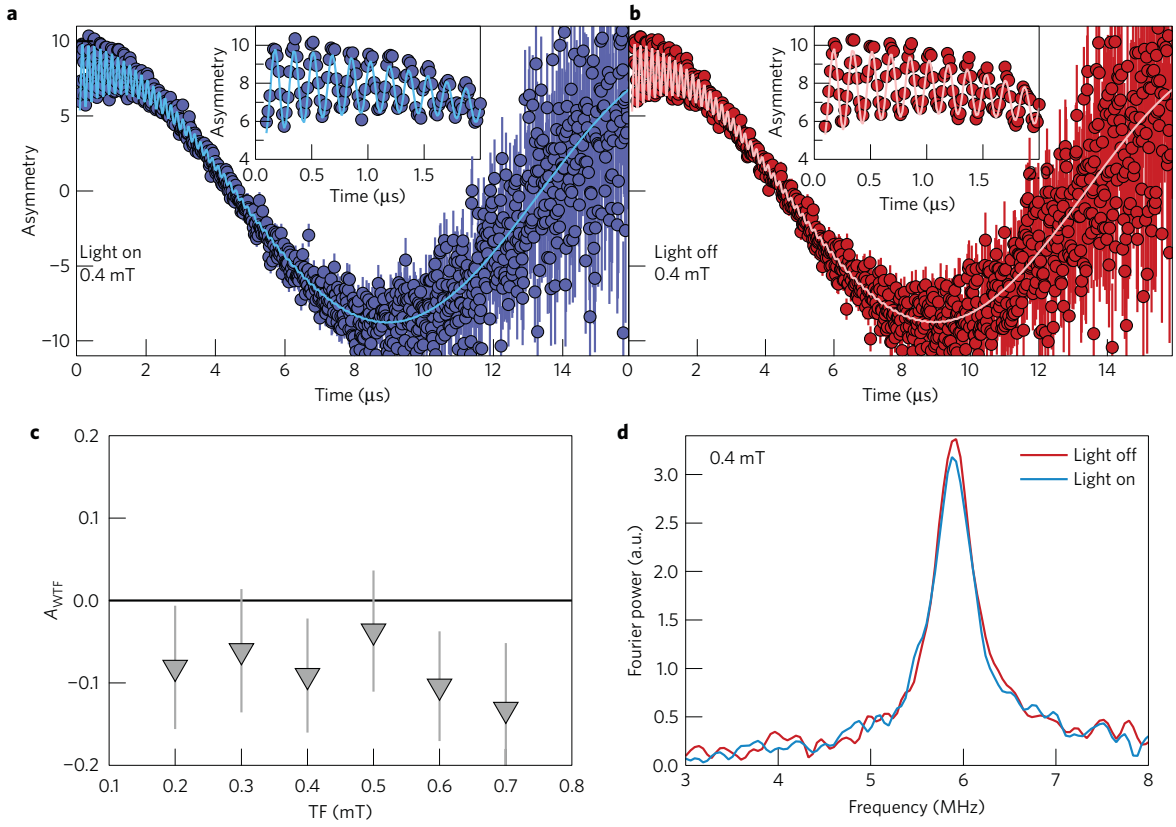

Figure 3 | A variety of muon measurements undertaken to understand the increase in amplitude of the ALC at low times. a,**b**, Weak transverse field data for light on (blue) $T_L = 130$ ns (**a**) and light off (red) (**b**), demonstrating that diamagnetic muons (slow precession; main panel) and unbound solvated muonium (fast triplet precession; insets) are present. The data have been fit to a two-component model (see text) to extract light-induced amplitude changes to the two components. Errors were calculated by taking the square root of the number of events for each detector group, and propagated using standard error analysis under the assumption of the normal distribution. **c**, The light-induced change in amplitude of the triplet precession, $A_{WTF} = A_{mu(on)} - A_{mu(off)}$. At all fields measured, there is a net reduction in solvated muonium when excitations are present, and it appears to be field independent. Errors are propagated on the fitted parameters on the assumption of the normal distribution, and represent a 68% confidence interval (standard error). **d**, Fourier transforms of the data shown in **a**,**b**, further demonstrating a light-induced change in amplitude, commensurate with a loss of solvated muonium.

despite it not having an α-proton (see Supplementary Information). Moreover, the larger dynamics present in bound muonium and the nuclear HFC significantly relaxes the triplet precession. All of these effects conspire together to make the radical triplet precession signal in a WTF all but invisible. However, changes in the solvated muonium amplitude, present if there is a light-induced change in reaction rate, are readily observable in the data upon fitting the spectra to $A(t) = A_{mu}\cos(\omega_{mu}t + \phi_{mu})\exp(-(\sigma_{mu}t)^2) + A_{\mu^+}\cos(\omega_{\mu^+}t + \phi_{\mu^+})\exp(-(\sigma_{\mu^+}t)^2)$. This represents a Gaussian-damped precession of the triplet muonium (first term) and spin precession in the applied field of the diamagnetic muons (second term), from which the light-induced change in the triplet precession asymmetry, $A_{WTF} = A_{mu(on)} - A_{mu(off)}$, is extracted. Figure 3c shows A_{WTF} with $T_L = 130$ ns, for several WTFs. All show a reduction in asymmetry of the triplet precession signal under photo-excitation, and this reduction appears to be field independent within error. This change is also present in the Fourier transforms of the data, an example of which is shown in Fig. 3d (see Supplementary Fig. 5 for all the Fourier transforms). This is clear evidence that there is an overall reduction in the amount of solvated muonium present following photo-excitation, which is consistent with an increased reaction rate of the solvated muonium with the molecule following excitation.

This conclusion has some implications about the timescales. If the reaction rate is comparable with the solvated muonium hyperfine frequency, then the shape of the longitudinal field (LF) repolarization curve is strongly governed by the reaction rate, as the muon partially exchanges spin polarization with the electron before forming the radical. However, the ALC amplitude is almost independent of reaction rate, since at high fields the muon's spin should be nearly or fully repolarized. Clearly, we are not in this fast regime. If, on the other hand, the inverse reaction rate approaches the lifetime of the muon (in excess of ∼100 ns), then the ALC amplitude is dependent on the reaction rate, as some muons will decay and be measured before they have a chance to react. Moreover, in this slow limit, there will be a clear two-step signature in the ground-state LF repolarization curve and only a weak light-induced effect in the intermediate field region of the LF repolarization. Both of these features are very clear in Fig. 4a,b. Importantly, the data shown in Fig. 4a correspond to a 10 mM solution of TIPS-Pn in DCM using a standard titanium cell mounted on an aluminium plate, on the EMU spectrometer at ISIS. Because of the materials used in this cell, the two-step repolarization curve, clearly evident in Fig. 4a, must be from the TIPS-Pn or DCM, and not the surrounding environment. This is strong evidence for either an entirely unreacted fraction of muonium, or a relatively slow reaction rate of muonium with the molecule.

Bringing all of the above information together, the light-induced changes to the ALC spectra in Fig. 2a are mainly related to a change in the reaction rate of the muonium with the molecule, specific to carbon 2. Whilst the mechanism of photodegradation in TIPS-Pn has not been fully clarified[35,36], it has previously been

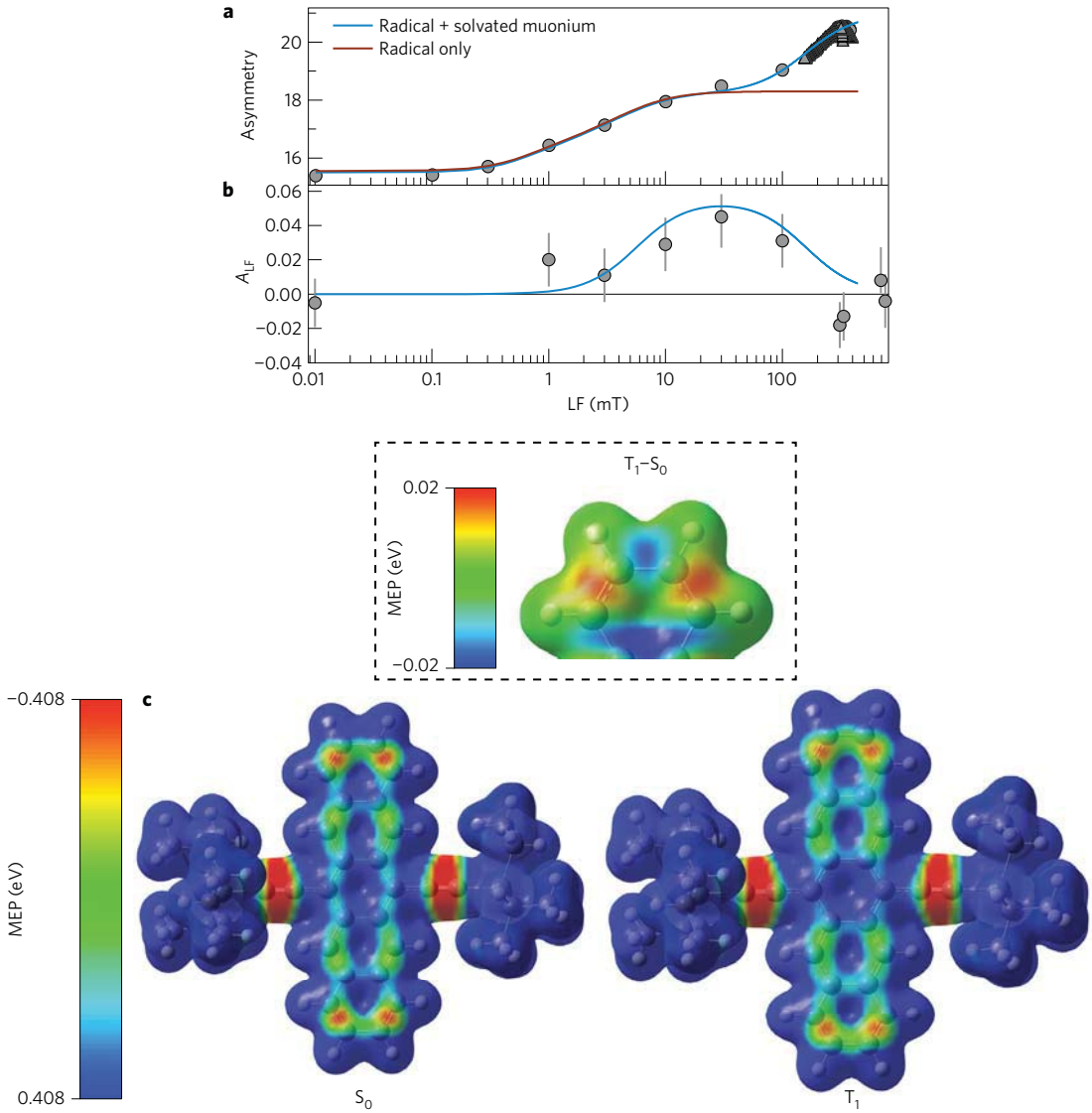

Figure 4 | Consistency checking with ground-state muon measurements. a, Longitudinal field repolarization data taken on the EMU spectrometer at ISIS in the ground state, using a well-characterized sample cell made from Ti. The data shows a clear two-step repolarization curve, corresponding to a radical fraction and solvated muonium. The lines correspond to the expected repolarization curve for just a radical (red) and a combined radical and solvated muonium state (blue). HFCs of 80 MHz and 4,463 MHz were used for radical and solvated muonium, respectively. Errors were calculated by taking the square root of the number of events for each detector group, and propagated using standard error analysis under the assumption of the normal distribution. **b**, The difference between the LF asymmetry for light on and off, $A_{LF} = A_{on} - A_{off}$, for $T_L = 130$ ns, using the HiFi spectrometer and the laser sample cell. A very small change at intermediate fields is present, which is consistent with a change in reaction rate dynamics in the slow limit or overall population reduction of the solvated muonium (see text). The line is a guide to the eye, representing the functional form expected from light-induced changes. Errors were calculated by taking the square root of the number of events for each detector group, and propagated using standard error analysis under the assumption of a normal distribution. **c**, The electrostatic potential map of the ground state S_0 and triplet excited state T_1 generated from DFT calculations (see text). On the end of the backbone, the charge is more spread when the triplet is present, resulting in a reduction in charge around the bond between carbons 1 and 2. This is most easily demonstrated by plotting the difference between T_1 and S_0, which is shown in the top centre of **c**. Here, the colour scale is amplified by a factor of 20, such that the red regions demonstrate a reduction in electron density of about 5%, and blue corresponds to an increase in electron density of about 5%.

inferred that TIPS-Pn undergoes a photoinduced inter-molecular 4 + 4 cycloaddition via a π-dimerization process[35]. However, we see little evidence for the reaction rate of muonium with site 4 being enhanced by excitation, probably because muonium chemistry is a good model for radical reactions, whereas dimerization of TIPS-Pn is an electrocyclic reaction.

Quantum chemical calculations were used to explore the electrostatic potentials that promote or inhibit molecular interactions, and to identify regions of the TIPS-Pn molecule with higher chemical reactivity. DFT was used with the B3LYP functional and cc-pVDZ basis set embedded in the Gaussian package[37]. After geometry optimization, the atomic charge distribution within the molecules along with its electronic volume was determined by a population analysis of the molecular orbitals. The surface enclosing 99% of the electronic density was calculated on a grid from the molecular orbital coefficients. The molecular electrostatic potential (MEP) was mapped[38] onto this surface (Fig. 4c) for both ground state and triplet state. The potential becomes significantly less negative around the bond between carbons 1 and 2 when the triplet excited state is present, as a

result of the electron density becoming more dispersed around the end ring of the backbone of the molecule. This is most easily observed by plotting the difference between the charge densities for T_1 and S_0 in the top panel of Fig. 4c, which shows that there is a reduction in the electron density between carbons 1 and 2 of approximately 5%. There are also changes to the electrostatic potential in the region of carbon 4, with a clear shift of electron density towards the centre of the molecule from the bond between carbons 4 and 3. The change to carbon 4 is roughly symmetrical—such that there is no large change in the overall electron density of the two bonds around carbon 4. This, coupled with steric hindrance of the side groups, may explain why there are no light-induced effects to the ALC associated with carbon 4. In addition to the changes to the electric potential governing chemical reactivity, there may also be a spin effect. It is likely that the muoniated molecule is in a doublet state, provided the spin of the muonium electron is opposite to the spin of the triplet already present. It is currently unknown what effect this will have on reactivity. The quartet state would result in the muonium electron residing in a higher-energy orbital, which would probably reduce the overall reactivity.

Molecular excited states and photochemical timescales

We now discuss the timescales presented in Fig. 2c. Recently, it has been shown that triplet–triplet dimers formed in TIPS-Pn dissolved in chloroform have an emission lifetime of approximately 220 ns (ref. 39). Whilst the 1 μs photo-μSR signal and this 220 ns dimer lifetime differ by a factor of over four, molecular interaction probabilities are strongly dependent on both concentration and solvent, as demonstrated by work on photodegradation[36], so it is feasible that dimerization processes are responsible for this timescale. Careful study of the transient absorption spectra reported by Walker *et al.*[39] for a concentration of 0.075 mol l^{-1} reveals a clear feature around 1.6 eV, also with a lifetime of approximately 1 μs. The onset of aggregate absorption in TIPS-Pn is 1.65 eV. Given this and the MEP discussed above, we suggest that the 1 μs photo-μSR component is related to an 'excimeric' process—that is, a species comprising two molecules, one in the ground state and the other in an excited state. The different electron densities of the ground state and triplet would probably promote a Coulomb-initiated 'excimer' state in TIPS-Pn, which presumably then leads to the eventual 4 + 4 cycloaddition at carbon 4, and a net increase in the muonium reactivity at carbon 2 while this state exists. Nonetheless, further study of this transient state with a 1 μs lifetime is necessary to properly identify it and its significance.

The 6.5 μs signal matches the triplet lifetime[39] and is therefore conclusive evidence that excited state processes can be measured with muoniated radicals with intra-molecular spatial resolution. Its amplitude has the opposite sign to the 1 μs signal, suggesting that it is directly related to a reduction in the reactivity of the muonium with the molecule, as a result of the reduced electron density in the carbon 2 bonds when the molecular excited state is present, as shown by the MEPs in Fig. 4c. This result, demonstrating that the time dependence of the excited state can be probed with an intra-molecular spatial resolution, is in itself quite remarkable. In principle, it should also be possible to image the time dependency of charge transfer states, in those systems where charge separation occurs in the excited state. Given the MEPs shown in Fig. 4c, it would be interesting to probe the central carbon atoms in TIPS-Pn, but unfortunately the relevant muonium bonding sites are blocked by the steric hindrance of the side groups.

Conclusions

We have demonstrated that reaction of muonium with an extended aromatic system can probe the relative levels of susceptibility of individual carbon atoms to chemical reaction upon excitation with light, and that this can be tracked as a function of time. We have presented evidence that a possible excited state with a 1 μs lifetime could be important to the photochemical degradation of TIPS-Pn in solution. This demonstrates the use of laser-pumped μSR and avoided level crossing resonances to gain insight into photochemical reactivity; clearly the technique has significant potential in other aromatic systems. We note that in TIPS-Pn, there are no polar species that would result in charge transfer states, so the changes to the electrostatic potential are relatively small. It would be interesting to extend this technique to molecules with such polar groups, where much larger changes to the electrostatic potential may be present, perhaps by either chemical modification of the TIPS-Pn backbone or by studying a known donor–acceptor molecule.

There is a second component that matches the triplet lifetime, 6.5 μs. This is strong evidence that muonium is able to map the time evolution of the excited state wavefunction on the molecule as a direct result of its sensitivity to electron density when reacting. This regioselectivity provides spatial resolution for studying excited state dynamics. To our knowledge, the experimental approach used here is the only one with this degree of temporal combined with direct intra-molecular spatial sensitivity; for example, typical resolutions in other mapping techniques are in excess of ten nanometres (refs 40,41). It may also be possible to extend the time window down to nano- or picoseconds with future technical developments. An experimental demonstration of these fast dynamics, we believe, will be an important step in the technique and, for a suitably chosen molecule, significant insight may be gained into the very fast photochemical and excited state processes at the molecular level.

Methods

Methods, including statements of data availability and any associated accession codes and references, are available in the online version of this paper.

Received 16 August 2016; accepted 31 October 2016; published online 12 December 2016

References

1. Singer, C. E. & Ames, B. N. Sunlight ultraviolet and bacterial DNA base ratios. *Science* **170,** 822–826 (1970).
2. Margulis, L., Walker, J. C. G. & Rambler, M. Reassessment of roles of oxygen and ultraviolet light in Precambrian evolution. *Nature* **264,** 620–624 (1976).
3. Jacobsen, E. N., Pfaltz, A. & Yamamoto, H. *Comprehensive Asymmetric Catalysis* (Springer, 1999).
4. Ojima, I. *Catalytic Asymmetric Synthesis* 3rd edn (Wiley, 2010).
5. Hoffmann, N. Photochemical reactions as key steps in organic synthesis. *Chem. Rev.* **108,** 1052–1103 (2008).
6. Lévesque, F. & Seeberger, P. H. Continuous-flow synthesis of the anti-malaria drug artemisinin. *Angew. Chem. Int. Ed.* **51,** 1706–1709 (2012).
7. Lunt, R. R., Giebink, N. C., Belak, A. A., Benziger, J. B. & Forrest, S. R. Exciton diffusion lengths of organic semiconductor thin films measured by spectrally resolved photoluminescence quenching. *J. Appl. Phys.* **105,** 053711 (2009).
8. Menke, S. M., Luhman, W. A. & Holmes, R. J. Tailored exciton diffusion in organic photovoltaic cells for enhanced power conversion efficiency. *Nat. Mater.* **12,** 152–157 (2013).
9. Hofmann, S., Rosenow, T. C., Gather, M. C., Lüssem, B. & Leo, K. Singlet exciton diffusion length in organic light-emitting diodes. *Phys. Rev. B* **85,** 245209 (2012).
10. High, A. A., Novitskaya, E. E., Butov, L. V., Hanson, M. & Gossard, A. C. Control of exciton fluxes in an excitonic integrated circuit. *Science* **321,** 229–231 (2008).
11. Hanna, M. C. & Nozik, A. J. Solar conversion efficiency of photovoltaic and photoelectrolysis cells with carrier multiplication absorbers. *J. Appl. Phys.* **100,** 074510 (2006).
12. Ehrler, B., Wilson, M. W., Rao, A., Friend, R. H. & Greenham, N. Singlet exciton fission-sensitized infrared quantum dot solar cells. *Nano Lett.* **12,** 1053–1057 (2012).
13. Congreve, D. N. *et al*. External quantum efficiency above 100% in a singlet-exciton-fission-based organic photovoltaic cell. *Science* **340,** 334–337 (2013).

14. Uoyama, H., Goushi, K., Shizu, K., Nomura, H. & Adachi, C. Highly efficient organic light-emitting diodes from delayed fluorescence. *Nature* **492,** 234–238 (2012).
15. Zhang, Q. *et al*. Efficient blue organic light-emitting diodes employing thermally activated delayed fluorescence. *Nat. Photon.* **8,** 326–332 (2014).
16. Green, M. A., Emery, K., Hishikawa, Y., Warta, W. & Dunlop, E. D. Solar cell efficiency tables (version 46). *Prog. Photovolt.* **23,** 1–9 (2015).
17. Schmidbauer, S., Hohenleutner, A. & König, B. Chemical degradation in organic light-emitting devices: mechanisms and implications for the design of new materials. *Adv. Mat.* **25,** 2114–2129 (2013).
18. Kondakov, D. Y., Brown, C. T., Pawlik, T. D. & Jarikov, V. V. Chemical reactivity of aromatic hydrocarbons and operational degradation of organic light-emitting diodes. *J. Appl. Phys.* **107,** 024507 (2010).
19. Yokoyama, K. *et al*. Future directions of μSR - laser excitation. *Phys. Scr.* **88,** 068511 (2013).
20. Kadono, R., Matsushita, A., Macrae, R. M., Nishiyama, K. & Nagamine, K. Muonium centers in crystalline Si and Ge under illumination. *Phys. Rev. Lett.* **73,** 2724–2727 (1994).
21. Ghandi, K., Clark, I. P., Lordc, J. S. & Cottrell, S. P. Laser-muon spin spectroscopy in liquids—A technique to study the excited state chemistry of transients. *Phys. Chem. Chem. Phys.* **9,** 353–359 (2007).
22. Nuccio, L., Schulz, L. & Drew, A. J. Muon spin spectroscopy: magnetism, soft matter and the bridge between the two. *J. Phys. D* **47,** 473001 (2014).
23. Fleming, D. G. *et al*. Kinetic isotope effects for the reactions of muonic helium and muonium with H_2. *Science* **331,** 448–450 (2011).
24. Baer, S., Fleming, D., Arseneau, D., Senba, M. & Gonzalez, A. Kinetic isotope effects in gas-phase muonium reactions. *ACS Symp. Ser.* **502,** 111–137 (1992).
25. Tanaka, T. & Takayanagi, T. Quantum reactive scattering calculations of H + F_2 and Mu + F_2 reactions on a new *ab initio* potential energy surface. *Chem. Phys. Lett.* **496,** 248–253 (2010).
26. Claxton, T. A. Aspects of muonium chemistry. *Chem. Soc. Rev.* **24,** 437–448 (1995).
27. Patterson, B. Muonium states in semiconductors. *Rev. Mod. Phys.* **60,** 69–159 (1988).
28. Kreitzman, S. R. & Roduner, E. Theory of avoided level-crossing relaxation dynamics for axial muonated radicals. *Chem. Phys.* **192,** 189–230 (1995).
29. Roduner, E. *The Positive Muon as a Probe in Free Radical Chemistry: Potential and Limitations of the μSR Techniques* (Springer, 1988).
30. Shimomura, K. *et al*. Pilot experiment for muonium photo ionization in GaAs. *J. Phys. Conf. Ser.* **225,** 012004 (2010).
31. Rhodes, C. J. Muonium—the second radioisotope of hydrogen—and its contribution to free-radical chemistry. *J. Chem. Soc. Perkin Trans.* **2,** 1379–1396 (2002).
32. Schulz, L. *et al*. Importance of intramolecular electron spin relaxation in small molecule semiconductors. *Phys. Rev. B* **84,** 085209 (2011).
33. Nuccio, L. *et al*. Importance of spin-orbit interaction for the electron spin relaxation in organic semiconductors. *Phys. Rev. Lett.* **110,** 216602 (2013).
34. Semba, M. Muon charge exchange and muonium spin exchange in gases. *Hyperfine Interact.* **65,** 779 (1991).
35. Coppo, P. & Yeates, S. G. Shining light on a pentacene derivative: the role of photoinduced cycloadditions. *Adv. Mater.* **17,** 3001–3005 (2005).
36. Abu-Sen, L., Morrison, J. J., Horn, A. B. & Yeates, S. G. Concentration- and solvent-dependent photochemical instability of 6,13-Bis(triisopropysilylethynyl)pentacene. *Adv. Opt. Mater.* **2,** 636–640 (2014).
37. Frisch, M. J. *et al*. *Gaussian09 Revision C.01* (Gaussian, 2010).
38. Murray, J. S. & Politzer, P. Statistical analysis of the molecular surface electrostatic potential: an approach to describing noncovalent interactions in condensed phases. *J. Mol. Struct.* **425,** 107–114 (1998).
39. Walker, B. J., Musser, A. J., Beljonne, D. & Friend, R. H. Singlet exciton fission in solution. *Nat. Chem.* **5,** 1019–1024 (2013).
40. Akselrod, G. M. *et al*. Visualization of exciton transport in ordered and disordered molecular solids. *Nat. Commun.* **5,** 3646 (2014).
41. Lunt, R. R. *et al*. Exciton diffusion lengths of organic semiconductor thin films measured by spectrally resolved photoluminescence quenching. *J. Appl. Phys.* **105,** 053711 (2009).

Acknowledgements

A.J.D. would like to acknowledge financial support from the European Research Council (MuSES project, proposal number 307593) and Sichuan University. All authors would like to acknowledge the scientific and technical support provided by the ISIS pulsed muon and neutron source. We would like to acknowledge Litron Lasers Ltd., as this work would not have been possible without their exceptional customer service and technical expertise. K.W. was funded by the Chinese Scholarship Council. P.M. was funded by Queen Mary University of London, under the Principal's Studentship scheme.

Author contributions

K.W. and P.M. contributed equally to this work. K.W., P.M., K.Y., J.S.L., F.L.P., J.H., L.S., M.W., N.A.M., S.Z., P.H. and A.J.D. performed the experimental work. K.Y., P.M., J.S.L. and A.J.D. designed, built, tested and commissioned the photo-μSR spectrometer (to be described fully elsewhere). P.M., K.Y., J.S.L., L.N., D.J.D., K.S., I.W., P.H. and A.J.D. set up the experimental equipment for the work reported here. K.W., J.S.L. and A.J.D. analysed and interpreted the μSR data. K.W. and A.M. performed the DFT calculations. J.E.A., P.H. and A.J.D. interpreted the implications of the results. Everyone contributed to writing the paper. A.J.D. conceived the research and managed the project.

Additional information

Supplementary information is available Correspondence and requests for materials should be addressed to P.H. or A.J.D.

Competing financial interests

The authors declare no competing financial interests.

Methods

The MuSES project, funded by the European Research Council, recently upgraded the HiFi spectrometer at ISIS to include a tunable, high-power laser system and associated infrastructure to perform light-pumped, muon-probed measurements. The sample was illuminated with 532 nm light from a 25 Hz Nd-YAG laser, with a pulse energy of 91 mJ. The fundamental frequency of ISIS is 50 Hz, so alternate light-on and light-off measurements were gated to different histograms (see Fig. 1). The laser system is housed in a light-tight cabin to the side of the HiFi spectrometer, and is routed underneath the floor to the beam entry chambers. The laser beam, after leaving the cabin, was routed toward the instrument by broadband dielectric mirrors (BBDM series from Semrock). The laser was aligned to a target mounted on the cold finger of closed cycle helium refrigerator (CCR), which indicates the centre of the muon beam. The muon beam position was confirmed with a fixed-point charge-coupled device (CCD) camera. The laser pulse was synchronized with the muon pulse using a digital delay generator (Stanford Research Systems, DG645), which triggers the YAG flashlamp and Q-switch with a set time delay. The trigger is defined from the proton extract kicker, either the current pulse or previous pulse, depending on the delay time needed (the crossover between these modes was $\sim$3.5 μs).
A liquid cell was designed to allow continuous flow of the solution through the illuminated area, such that the sample is replaced (from a large bath via a peristaltic pump with polytetrafluroethylene (PTFE) tubing) to minimize the effect of any photochemical reactions that may occur. The flow rate was set to approximately 0.1 ml s^{-1}. The solvent was degassed via a standard freeze–pump–thaw method prior to dissolving the solute, and the entire circulation system was contained in an argon atmosphere for the duration of the experiment. A 10 mM solution concentration was decided upon by factoring in the muoniated radical formation probability, singlet fission quantum efficiency and light absorption length at the chosen wavelength (532 nm). Further technical details of the new experimental set-up are summarized more fully in the Supplementary Information. Details on the muon technique, and further references, can be found in several articles[22,23,27,28].

The conformational study and subsequent muonium site assignment was performed using DFT using the Gaussian 09 package, and taken at the theory level of B3LYP/DGDZVP. This produces a relatively accurate results for the ALC resonant fields for TIPS-Pn (see Supplementary Information).

Data availability. Raw experimental data is available on a publicly accessible repository (http://data.isis.stfc.ac.uk). Analysed data shown in the figures and DFT calculations will be made available upon request to the corresponding authors.